Theor Chem Acc (2005) 114: 159–168
DOI 10.1007/s00214-005-0657-9

REGULAR ARTICLE

A.H.C. Horn · Jr-H. Lin · T. Clark

Multipole electrostatic model for MNDO-like techniques with minimal valence *spd*-basis sets

Received: 30 August 2004 / Accepted: 27 October 2004 / Published online: 15 July 2005

Abstract We report an implementation of an atomic multipole model (up to quadrupole) for calculating the electrostatic properties of molecules based on electron densities derived from MNDO-like NDDO-based semiempirical MO calculations with minimal *s*,*p*,*d* valence basis sets. The results were validated by a comparison of the calculated values of the molecular electrostatic potential with those obtained from fine grain numerical integrations (both with AM1*), B3LYP/6–31G(d) and MP2/6–31G(d). The DFT and ab initio potentials can be reproduced remarkably well (mean unsigned error $<2\,\mathrm{kcal\,mol^{-1}\ e^{-1}}$) using simple linear regression equations to correct the AM1* (multipole) results.

1 Introduction

Coulomb interactions are usually the major contribution to intermolecular interaction energies [1]. The molecular electrostatic potential (MEP) [2] has thus played an important role in applications that depend on intermolecular interaction energies, such as quantitative structure-activity (QSAR), [3] and -property (QSPR) [4] relationships, prediction of toxicity [5], docking [6], (continuum) solvation models [7–10] and many others. The MEP can be derived from the results of quantum mechanical calculations using

$$\mathrm{MEP}(\mathbf{r}) = \sum_{i=1}^{n} \frac{Z_i}{|\mathbf{R}_i - \mathbf{r}|} - \int_{-\infty}^{\infty} \frac{\rho(\mathbf{r}')}{|\mathbf{r}' - \mathbf{r}|}\,\mathrm{d}\,\mathbf{r}'\,, \qquad (1)$$

where n is the number of atoms in the molecule, Z_i is the nuclear charge of atom i located at $\mathbf{R}_i$ and $\rho(\mathbf{r})$ is the electron density of the molecule.

Equation 1, however, involves integration of the electron density, which is computationally acceptable within the framework of ab initio or density-functional theory (DFT) calculations, but becomes prohibitively expensive in comparison with the calculation of the wavefunction for semiempirical molecular orbital (MO) calculations such as those using the MNDO, [11] AM1 [12] or PM3 [13] Hamiltonians. The increasing use of such techniques for large numbers of molecules in cheminformatics applications [14] requires not only fast accurate calculations of the MEP, but also a compact representation of the electrostatics of the molecule that can be stored efficiently for reuse.

Several groups have therefore proposed techniques for calculating the MEP from semiempirical wavefunctions. Rein [15] investigated the use of multipoles up to quadrupoles with semiempirical techniques as early as 1973. Merz and Besler [16] used a transformation to contracted Gaussian functions in MOPAC-ESP to circumvent the computationally difficult problem of calculating integrals over Slater atomic orbitals (AO), which are used as the basis set in most MNDO-like techniques. However, the calculational task remains very significant in comparison with the energy calculation so that this technique is no longer popular. Reynolds et al.[17] pointed out that the MEP can be calculated with little loss in accuracy by applying the zero-differential overlap (ZDO) [18] approximation strictly (i.e.by ignoring the two-atom blocks of the density matrix). They explicitely calculated the one-electron integrals using *s*- and *p*-Slater basis functions. A similar ZDO approach was taken by Ford and Wang [19] and later by Bakowies and Thiel [20]. Their technique used the multipole approximation for two-electron integrals introduced by Dewar and Thiel [21] for MNDO to compute (and scale) the one-electron integrals.

We used the fact that hybrid atomic orbitals (HAOs) can be described by one variable, the *s*-coefficient, within a minimal valence *sp*-basis set to define the computationally efficient natural atomic orbital/point charge (NAO-PC) model

Dedicated to Prof. Karl Jug on the occasion of his 65th birthday

A.H.C. Horn · Jr-H. Lin · T. Clark (✉)
Computer-Chemie-Centrum,
Friedrich-Alexander-Universität Erlangen-Nürnberg,
Nägelsbachstraße 25, 91052 Erlangen, Germany.
E-mail: clark@chemie.uni-erlangen.de

A.H.C. Horn
Bioinformatik, Institut für Biochemie,
Friedrich-Alexander-Universität Erlangen-Nürnberg,
Fahrstraße 17, 91054 Erlangen, Germany.

[22–25]. In this technique, the natural atomic orbitals (NAOs) [26] are represented by two negative point charges, one located at the charge center of each orbital lobe. This model circumvents the integration step by precomputing the dependence of the position and magnitude of the charges on the *s*-coefficient of the NAO from high-resolution numerical integrations of the Slater AO. The NAO-PC model, however, has two drawbacks. Because the NAOs are derived by diagonalization of the one-atom blocks of the density matrix, ones with degenerate occupancies are not given uniquely, leading to erroneous results as found, for instance, for fullerenes [27]. This problem can be avoided using alternative models based on HAOs or localized MOs [27]. The second problem, however, means that the NAO-PC technique cannot be extended easily to methods that use *d*-orbitals in the basis set. This difficulty arises because the HAOs are no longer defined by the *s*-coefficient, so that multidimensional lookup functions would be necessary for *spd*-basis sets.

In order to resolve the above difficulties, we have returned to the ZDO-approach of Reynolds et al. (NAO-PC is also a ZDO-technique) and have formulated it in terms of an atom-multipole model similar to that also derived from the NAO-PC charges [23]. Because the two-center integrals in MNDO [11] and MNDO/d [28,29] are calculated within a multipole approximation limited to monopoles, dipoles and quadrupoles, the one-atom blocks of the density matrix can be represented directly as linear combinations of the multipoles corresponding to the individual charge distributions. The sum of these multipoles then gives the atomic monopole (equivalent to the Coulson charge), dipole and quadrupole. This allows us to store a representation of the anisotropic atomic electron density as ten floating-point numbers (the monopole, three components of the dipole vector and six components of the symmetrical quadrupole tensor).

We now describe an implementation of this technique. In the appendices, we list the charge arrays representing each charge distribution for a minimal valence *spd*-basis set and give the formulae used to calculate the MEP and the electrostatic field from the atomic multipoles. These formulae have been given before [11,28,29] but we collect them all together here for convenience in future applications.

2 Theory

2.1 Treatment of two-electron integrals in MNDO-like semiempirical methods

MNDO-type semiempirical methods use Slater–Zener orbitals as their basis set. These AO ϕ with quantum numbers n, l, m are defined in the usual manner [30]. They can be separated into a radial function $R_{nl}(r)$ and a normalized spherical harmonic part $S_{lm}(\Theta, \Phi)$ [31] according to

$$\phi_{nlm} = R_{nl}(r)\, S_{lm}(\Theta, \Phi)\,. \tag{2}$$

However, the Slater–Zener basis functions are not used directly for integral evaluation in semiempirical programs because of the complexity of the mathematical expressions.

Instead, an elegant simplification[11] is used, in particular, for the two-electron integrals $(\mu\nu|\lambda\sigma)$ (Eq. 3; e is the electronic charge, r_{12} is the interelectronic distance and $d\tau_1$ and $d\tau_2$ denote the integration volume elements over the coordinates of electron 1 and 2):

$$(\mu\nu|\lambda\sigma) = \int\int \phi_\mu(1)\phi_\nu(1)\frac{e^2}{r_{12}}\phi_\lambda(2)\phi_\sigma(2)\,\mathrm{d}\tau_1\,\mathrm{d}\tau_2\,. \tag{3}$$

In the NDDO-approximation[32] the three- and four-center two-electron integrals are neglected; the remaining two-center two-electron integrals $(\mu^A\nu^A|\lambda^B\sigma^B)$ describe the electrostatic interaction between the two-charge distributions $\rho^{\mu\nu}(1) = \mu\nu$ and $\rho^{\lambda\sigma}(1) = \lambda\sigma$ on the atomic centers A and B. Because such a charge distribution ρ can be expressed in terms of a finite linear combination of normalized real spherical harmonics, the real spherical multipole moment components of ρ may be written as [28,31]

$$\begin{aligned} M_{lm}^{\mu\nu} &= \int \mathrm{d}_{lm}\, r'\, S_{lm}(\Theta, \Phi)\, \rho^{\mu\nu}(r, \Theta, \Phi)\,\mathrm{d}\tau \\ &= e\, a_{lm}^{\mu\nu}\, \mathrm{d}_{lm} \int R_{n_\mu l_\mu}(r)\, R_{n_\nu l_\nu}(r)\, r^{l+2}\,\mathrm{d}r \\ &= e\, a_{lm}^{\mu\nu}\, \mathrm{d}_{lm}\, A_l^{\mu\nu}\,, \end{aligned} \tag{4}$$

with

$$\mathrm{d}_{lm} = \sqrt{\frac{4\pi}{2l+1}}, \tag{5}$$

$$\begin{aligned} A_l^{\mu\nu} &= (2\zeta_\mu)^{n_\mu+1/2}\,(2\zeta_\nu)^{n_\nu+1/2}(\zeta_\mu+\zeta_\nu)^{-n_\mu-n_\nu-l-1} \\ &\quad\times\frac{(n_\mu+n_\nu+l)!}{\sqrt{(2n_\mu)!(2n_\nu)!}}\,. \end{aligned} \tag{6}$$

where we use the orthogonality of the spherical harmonics to simplify the expressions.The coefficients $a_{lm}^{\mu\nu}$ in Eq. (4) are related to the Clebsch–Gordan coefficients (see reference [28] for details); ζ_μ and ζ_ν (Eq. 5) are the orbital exponents from the radial part of the Slater–Zener orbitals:

$$R_{nl}(r) = \frac{(2\zeta)^{n+1/2}}{(2n)!^{1/2}}\, r^{n-1}\, \mathrm{e}^{-\zeta r} \tag{7}$$

With the expressions in Eq. 4 the two-center two-electron integral $(\mu\nu|\lambda\sigma)$ can be calculated as a sum over classical multipole interactions. However, this classical description breaks down for small interatomic distances, where the two interacting charge distributions $\rho^{\mu\nu}$ and $\rho^{\lambda\sigma}$ overlap. Thus, the multipole interaction $[M_{l_1m}^{\mu\nu}, M_{l_2m}^{\lambda\sigma}]$ is modified by applying the Klopman formula [33] to each interaction between the point charges describing the two interacting multipoles, so that the final formula for computing the two-center two-electron integrals reads[28]

$$(\mu\nu|\lambda\sigma) = \sum_{l_1,l_2}\sum_{m=-l_{\min}}^{l_{\min}} [M_{l_1m}^{\mu\nu}, M_{l_2m}^{\lambda\sigma}]\,, \tag{8}$$

where $l_{\min}$ is the smaller of l_1 and l_2. In MNDO-like methods the one-electron integrals are also calculated using this approach (i.e. as if they were two-electron integrals in which one charge distribution is a point charge).

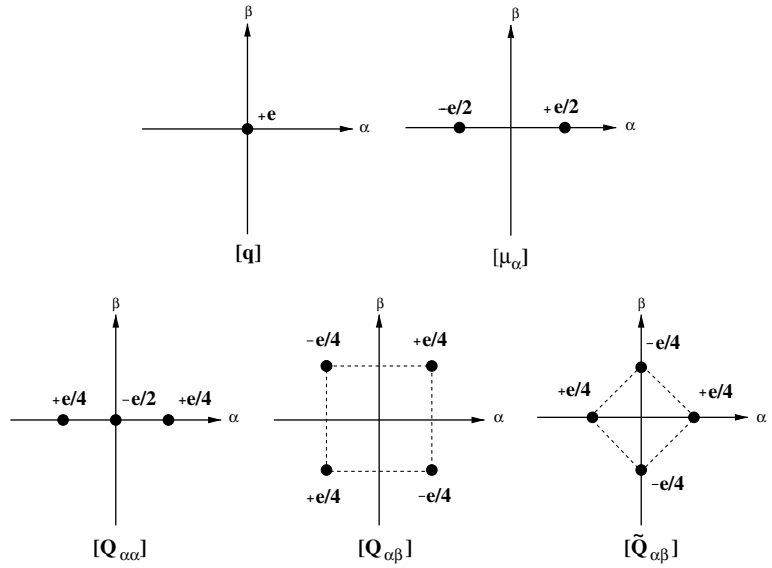

Fig. 1 Point-charge configurations ($\alpha, \beta = x, y, z$). The separation between two neighboring point charges of opposite sign is 2 D (cf Table 2)

A minimal spd basis yields 45 unique charge distributions $\mu\nu$ (1 ss, 3 sp, 5 sd, 6 pp, 15 pd and 15 dd) with 96 nonvanishing multipole moments $M_{lm}^{\mu\nu}$. However, for practical reasons, the 44 octopole and hexadecapole moments are neglected, only monopoles, dipoles and quadrupoles are kept. These have been shown in numerical test calculations to reproduce the major contributions to the interaction [28].

The point-charge configurations arising from the multipoles up to $l = 2$ are shown schematically in Fig. 1, where the separation between two adjacent point charges of opposite sign is $2D$ (see ref [28,29] for details). Table 2 in the Appendix provides coordinates and charge values for the point charges of all possible charge configurations $\mu\nu$. Note that the magnitudes of charges for each charge configuration are given by the corresponding density matrix element $P_{\mu\nu}$.

The atomic charge, dipole and quadrupole moment can be calculated easily from this array of multipole point charges according to standard formulae [34].

2.2 Electrostatic potential caused by multipole charge distributions

Having defined the atom-based multipoles in the framework of semiempirical MO theory, we can now use them to calculate molecular properties. The MEP at a point **r** caused by multipoles is defined in general according to Eq.(9),

$$\mathrm{MEP}(\mathbf{r}) = q\left(\frac{1}{R}\right) - \hat{\mu}_\alpha \nabla_\alpha \left(\frac{1}{R}\right) + \frac{1}{3}\hat{\Theta}_{\alpha\beta}\nabla_\alpha\nabla_\beta\left(\frac{1}{R}\right) - \cdots, \tag{9}$$

where q, $\hat{\mu}_\alpha$ and $\hat{\Theta}_{\alpha\beta}$ are the operators for monopole, dipole and quadrupole, respectively, R is the distance between the multipole center and the MEP point, and ∇ is the Nabla operator. Explicit formulae,[35] also for the electric field and the field gradient, are given in Appendix A.

Using the atom-based multipoles, the MEP at a certain point in space can now be calculated easily by summing up the charge, dipole and quadrupole contributions of all atoms.

3 Performance

In order to perform some preliminary tests, we have compared the multipole electrostatics to numerically computed semiempirical MEP values and to ab initio results. We chose a small test set of molecules (cf Fig. 2) that was geometry

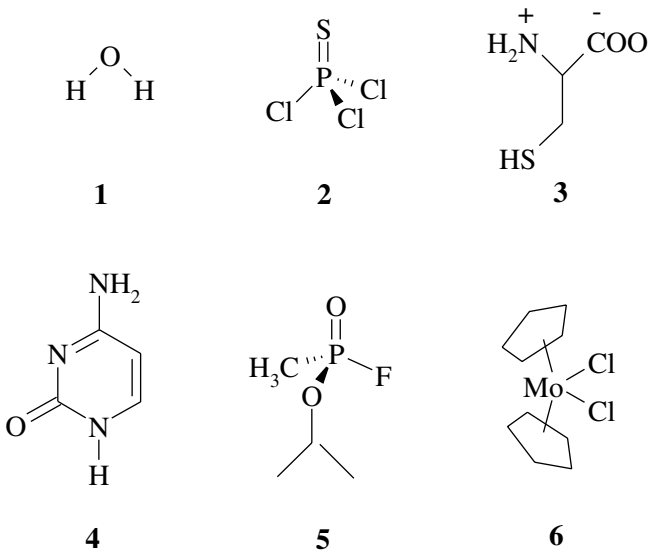

Fig. 2 The test set molecules

Table 1 Overview of test set computed with AM1*

Number	Sum formula	Symmetry	Hamiltonian	Basis functions	ESP points
1	H_2O	C_{2v}	AM1	6	48
2	$SPCl_3$	C_{3v}	AM1*	45	79
3	$C_3O_2NH_7S$	C_1	AM1*	40	68
4	$C_4ON_3H_5$	C_s	AM1	41	82
5	$C_4O_2PFH_{10}$	C_1	AM1*	47	85
6	$C_{10}H_{10}Cl_2Mo$	C_{2v}	AM1*	77	72

optimized with VAMP[36] using the AM1* Hamiltonian[37] for molecules containing *d* elements. The structure obtained was then subjected to the different MEP computation methods.

For the numerical calculation of the electron density needed for the numerically computed MEP the molecule's solvent accessible surface was determined. To save computation time the symmetry of the molecule was taken into account so that, for example, for water just one-quarter of the surface points was used for the MEP calculation. For the numerical integration the molecule was surrounded by a point grid with a minimal distance of 30 Å from an atom to the grid border; the grid density was set to 15 $Å^{-1}$. Table 1 summarizes the number of surface points for each molecule of the test set finally used for the MEP computation.

We also compared the semiempirical MEPs with B3LYP [38,39] and Moller-Plesset second-order (MP2)[40–43] results, in order to judge their accuracy.We used the 6-31G(d) basis set [44–46] throughout. For Molybdenum (molecule 6), the LANL2DZ basis set with Los Alamos pseudopotentials [47–49] and with additional polarization functions [50] was used. All ab initio calculations were performed using the Gaussian03 program package[51].

Figures 3–7 show the ESP results of the two semiempirical and the two ab initio methods (all values are in kcal mol^{-1} e^{-1}).

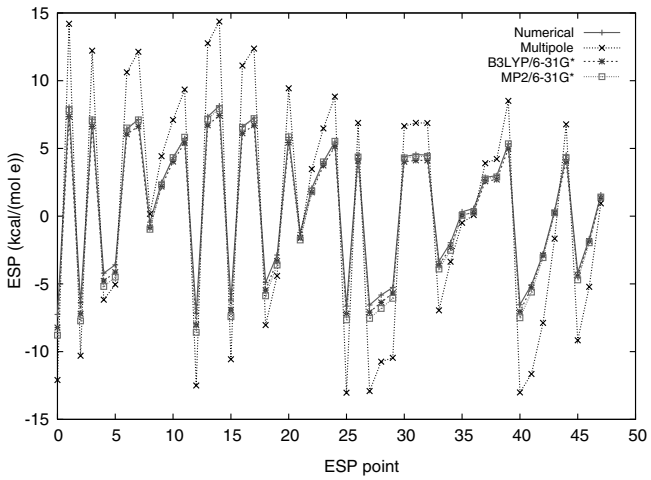

Fig. 3 Water: ESP on the symmetrized solvent-accessible surface

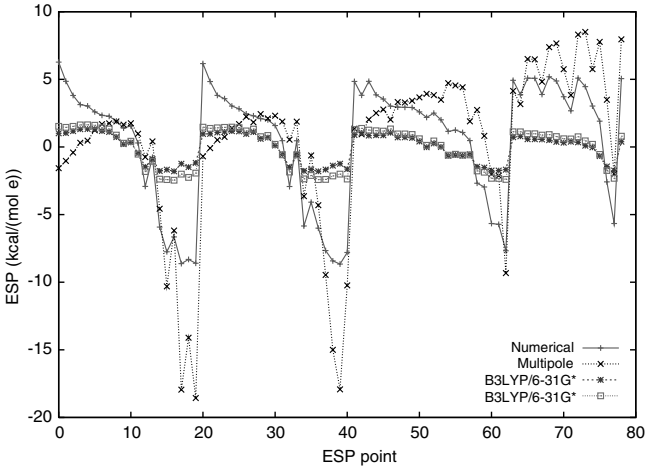

Fig. 4 $SPCl_3$: ESP on the symmetrized solvent-accessible surface

3.1 Comparison to numerical ESP calculation

With one exception, the multipole ESP reproduces the shape of the numerical ESP curve well. However, the agreement is less good for compound 2 ($SPCl_3$).Generally, however, the multipole method gives ESP values whose absolute magnitude is symmetrically too high. Again, compound 2 can be considered an exception, in which the numerical ESP curve shows three local maxima with higher values than the three other curves.

3.2 Comparison to *ab initio* ESP Calculation

Figures 3–7 show that the difference between the two ab initio ESP values and the semiempirical ones is small, although MP2 yields slightly larger absolute values than DFT, as expected.

Again, apart from compound 2, the semiempirical ESP curves reflect their ab initio counterparts in shape (Fig. 8). The

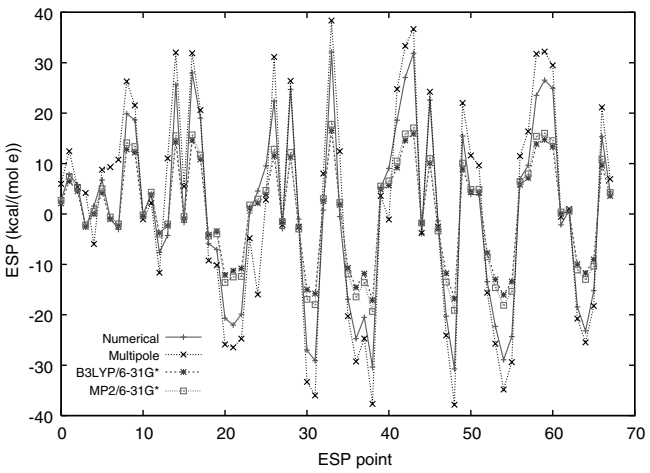

Fig. 5 Cysteine zwitterion: ESP on the solvent-accessible surface

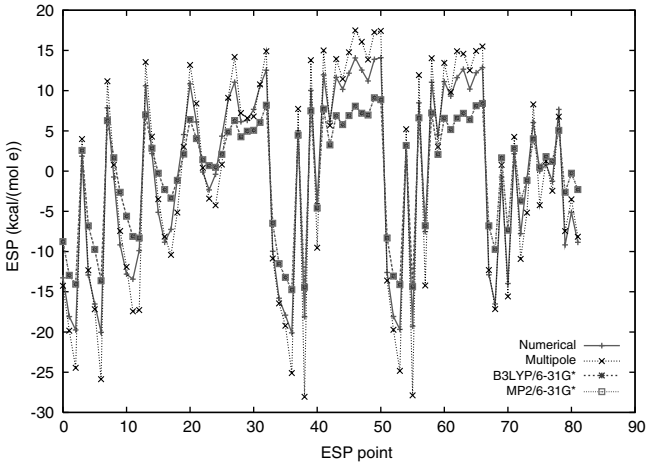

Fig. 6 Cytosine: ESP on the symmetrized solvent-accessible surface

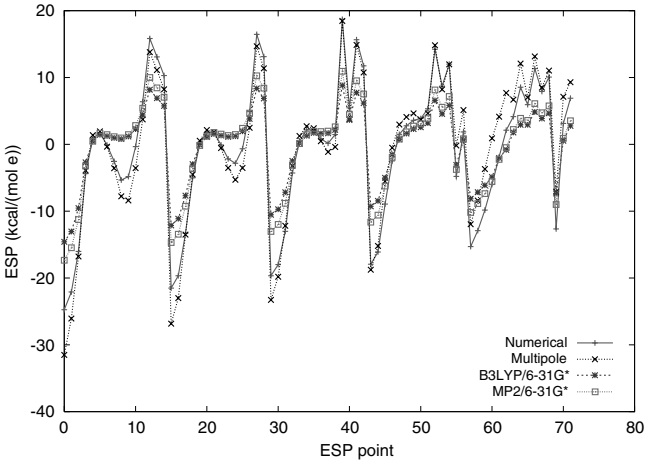

Fig. 8 $MoCp_2Cl_2$: ESP on the symmetrized solvent-accessible surface

values differ systematically, that is, the absolute numerical ESP values are larger than the ab initio ones, but smaller than those calculated by the multipole method.

3.3 General correlation

Although we did not expect a perfect correlation between the multipole ESP method and other techniques, especially not with the ab initio results, we have investigated the relationships between the values obtained with the different methods. Thus, we plotted the multipole ESP values of all molecules against those of the other methods. To quantify the relationship between the ESP values we computed the Carbo[52], S_{XY}^{Carbo}, and Hodgkin[53], S_{XY}^{Hodgkin}, indices as well as the Pearson correlation coefficient, r_{XY}, according to Eqs (10), (11) and (12).

$$S_{XY}^{\text{Carbo}} = \frac{\sum_{i=1}^{n} x_i y_i}{\sqrt{\sum_{i=1}^{n} x_i^2 + \sqrt{\sum_{i=1}^{n} y_i^2}}} \tag{10}$$

$$S_{XY}^{\text{Hodgkin}} = \frac{2\ \sum_{i=1}^{n} x_i y_i}{\sum_{i=1}^{n} x_i^2 + \sum_{i=1}^{n} y_i^2} \tag{11}$$

$$r_{XY} = \frac{\sum_{i=1}^{n} (x_i - \bar{x})(y_i - \bar{y})}{\sqrt{\sum_{i=1}^{n} (x_i - \bar{x})^2 \sum_{i=1}^{n} (y_i - \bar{y})^2}} \tag{12}$$

Figure 9 shows the correlation between the multipole and the numerical ESP values for all 434 ESP surface points. The Carbo index is 0.965, the Hodgkin index to 0.963, and the correlation coefficient to 0.965.

The correlation between the multipole and DFT ESP calculations (Fig. 10) shows a systematic deviation, as also seen in Figs. 3–7. Thus, the similarity indices are still quite satisfactory: Carbo index 0.952, Hodgkin index 0.859, correlation coefficient 0.952, but the absolute values deviate significantly. Nevertheless, the DFT results are reproduced well by the regression equation Eq (13) (in kcal mol^{-1} e^{-1})

$$\text{ESP}_{\text{DFT}} = 0.463 \cdot \text{ESP}_{\text{AM1*}} - 0.028 \tag{13}$$

with $N = 434$, $r^2 = 0.907$, $\sigma = 1.9$ and MUE= 1.3.

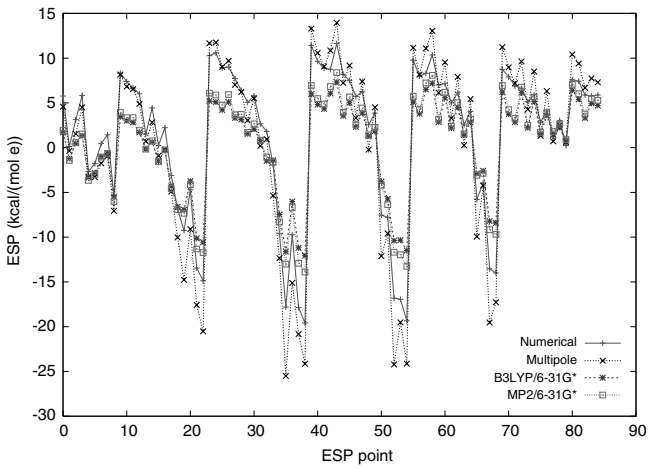

Fig. 7 Sarin ESP on the solvent-accessible surface

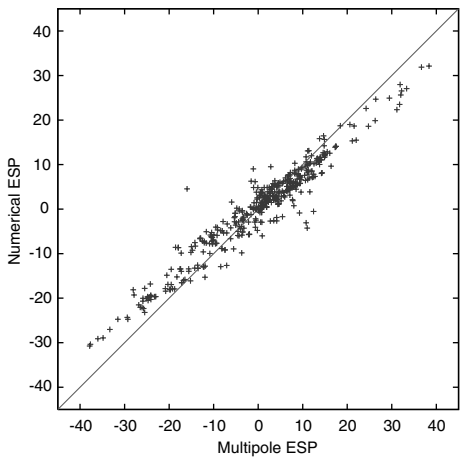

Fig. 9 Multipole versus Numerical ESP (ESP points of all test molecules included)

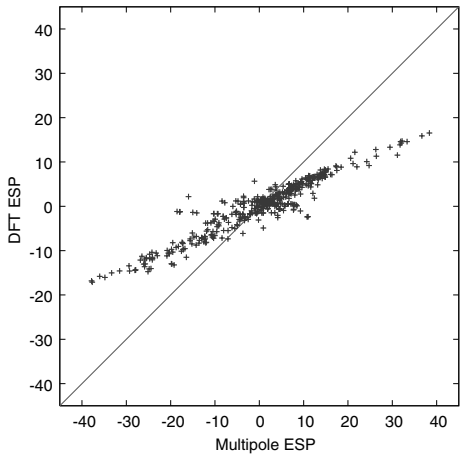

Fig. 10 Multipole versus DFT ESP (ESP points of all test molecules included)

The MP2 calculations (Fig. 11) give a similar picture to the DFT case. We clearly see a correlation that has also manifested itself in the different similarity indices. The Carbo index is now 0.952, the Hodgkin index 0.901 and the correlation coefficient 0.952. The regression equation for the MP2 results is given by Eq (14) (again, in kcal mol^{-1} e^{-1})

$$\mathrm{ESP_{MP2}} = 0.525 \cdot \mathrm{ESP_{AM1*}} - 0.009 \qquad (14)$$

with $N = 434$, $r^2 = 0.907$, $\sigma = 2.1$ and MUE= 1.5.

4 Summary and outlook

We have presented a new method for the calculation of molecular electrostatic properties in the spirit of NDDO semiempirical methods based on a multipole-interaction scheme. The atom-based monopole, dipole and quadrupole moments are computed from the point-charge sets used to calculate the two-electron integrals in MNDO-type methods[21].

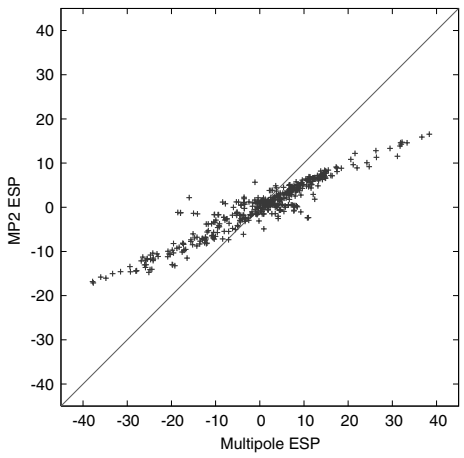

Fig. 11 Multipole versus MP2 ESP (ESP points of all test molecules included)

Although the new method gives systematic deviations from the numerical AM1*-ESP, and especially B3LYP/6-31G(d) and MP2/6-31G(d) calculations, the overall performance is very encouraging. B3LYP/6-31G(d) and MP2/6-31G(d) ESP values can be reproduced with mean unsigned errors under 2 kcal mol^{-1} e^{-1} using the regression equations Eq (13) and (14), respectively. However, the fact that one compound of the test set ($SPCl_3$) exhibits distinct differences in ESP values might point to a common problem in semiempirical methods, the correct treatment of the core–core repulsion. Many NDDO methods use parameterized Gaussian functions to model the interaction between nuclei, an approach that is not guaranteed to work correctly for all cases [54].

However, we are convinced that our multipole ESP approach is a step in the right direction. Our next steps are the application of the method to the computation of the electric field in the framework of continuum solvent models and the definition of multipole-ESP derived atomic charges, comparable to our VESPA charges [55,56].

Acknowledgements The authors thank A.A. Voityuk for helpful comments and M. Hennemann for support with the Gaussian program. A.H.C. Horn thanks G.Wellein from the Regionales Rechenzentrum Erlangen for advice concerning the parallelization of the numerical ESP code.

Appendix A

In the standard coordinate system the following orbital-symmetry relations hold [21]:

$p_x = p_\pi$, $p_y = p_{\bar{\pi}}$, $p_z = p_\sigma$, $d_{z^2} = d_\sigma$, $d_{xz} = d_\pi$, $d_{yz} = d_{\bar{\pi}}$, $d_{x^2-y^2} = d_\delta$, $d_{xy} = d_{\bar{\delta}}$.

The following Table 2 gives all point charges for the multipole expressions arising from the electronic charge distributions $\mu\nu$ including the point-charge configuration coefficients; the quantities D^{sp}, D^{sd}, D^{pp}, D^{pd} and D^{dd} are atom specific constants and can be calculated in the usual way [28]. The multipole M_{00} represents a monopole $[q]$, and M_{10}, M_{11}, M_{1-1} a dipole $[\mu_\alpha]$. For charge distributions $p_\alpha p_\alpha$ and $p_\alpha p_\beta$, a linear quadrupole $[Q_{\alpha\alpha}]$ or square quadrupole $[Q_{\alpha\beta}]$ is adopted (M_{20}, M_{21}, M_{2-1}, M_{2-2}), respectively. Charge distributions involving d orbitals and the multipole moments M_{20} and M_{22} are represented by the quadrupole charge configurations $[Q_{xy}]$ or $[Q_{zx}] - \frac{1}{2}[Q_{xy}]$ (cf Fig. 1). Note that for the sp and pd dipole contributions, the expressions are simplified to an origin-based dipole vector. It should also be noted that for the calculation of the atomic monopole the core charge must be taken into account.

Appendix B

For the sake of completeness we repeat the general formulae from ref [35] for the MEP (Eq. (15)), the electric field (Eq.

Table 2 Point-charge arrays for the monoatomic charge distributions within a minimal valence *spd*-basis arising from the nonzero multipole moments $M_{lm}^{\mu\nu}$ up to quadrupoles for charge a distribution $\mu\nu$. The atom-specific distance abbreviations D_1^{sp}, D_1^{pd}, D_2^{sd}, D_2^{pd} and D_2^{dd} correspond to those defined in references [11] and [28]

μ	ν	l	m	N	x	y	z	q
s	s	0	0	1	0.0	0.0	0.0	+1
s	p_x	1	1	2	$+2\ D_1^{sp}$	0.0	0.0	+1
s	p_y	1	−1	2	0.0	$+2\ D_1^{sp}$	0.0	+1
s	p_z	1	0	2	0.0	0.0	$+2\ D_1^{sp}$	+1
s	d_{xy}	2	−2	4	$+D_2^{sd}$	$+D_2^{sd}$	0.0	+1/4
					$-D_2^{sd}$	$-D_2^{sd}$	0.0	+1/4
					$+D_2^{sd}$	$-D_2^{sd}$	0.0	−1/4
					$-D_2^{sd}$	$+D_2^{sd}$	0.0	−1/4
s	d_{yz}	2	−1	4	0.0	$+D_2^{sd}$	$+D_2^{sd}$	+1/4
					0.0	$-D_2^{sd}$	$-D_2^{sd}$	+1/4
					0.0	$+D_2^{sd}$	$-D_2^{sd}$	−1/4
					0.0	$-D_2^{sd}$	$+D_2^{sd}$	−1/4
s	d_{xz}	2	1	4	$+D_2^{sd}$	0.0	$+D_2^{sd}$	+1/4
					$-D_2^{sd}$	0.0	$-D_2^{sd}$	+1/4
					$+D_2^{sd}$	0.0	$-D_2^{sd}$	−1/4
					$-D_2^{sd}$	0.0	$+D_2^{sd}$	−1/4
s	d_{z^2}	2	0	6	0.0	0.0	$+\sqrt{2}\ D_2^{sd}$	$\sqrt{(4/3)}$ (+1/4)
					0.0	0.0	$-\sqrt{2}\ D_2^{sd}$	$\sqrt{(4/3)}$ (+1/4)
					$+\sqrt{2}\ D_2^{sd}$	0.0	0.0	$\sqrt{(4/3)}$ (−3/8)
					$-\sqrt{2}\ D_2^{sd}$	0.0	0.0	$\sqrt{(4/3)}$ (−3/8)
					0.0	$+\sqrt{2}\ D_2^{sd}$	0.0	$\sqrt{(4/3)}$ (+1/8)
					0.0	$-\sqrt{2}\ D_2^{sd}$	0.0	$\sqrt{(4/3)}$ (+1/8)
s	$d_{x^2-y^2}$	2	2	4	$+\sqrt{2}\ D_2^{sd}$	0.0	0.0	+1/4
					$-\sqrt{2}\ D_2^{sd}$	0.0	0.0	+1/4
					0.0	$+\sqrt{2}\ D_2^{sd}$	0.0	−1/4
					0.0	$-\sqrt{2}\ D_2^{sd}$	0.0	−1/4
p_x	p_x	0	0	1	0.0	0.0	0.0	+1
		2,2	0,2	3	$+2D_2^{pp}$	0.0	0.0	+1/4
					$-2D_2^{pp}$	0.0	0.0	+1/4
					0.0	0.0	0.0	−1/2
p_y	p_y	0	0	1	0.0	0.0	0.0	+1
		2,2	0,2	3	0.0	$+2D_2^{pp}$	0.0	+1/4
					0.0	$-2D_2^{pp}$	0.0	+1/4
					0.0	0.0	0.0	−1/2
p_z	p_z	0	0	1	0.0	0.0	0.0	+1
		2,2	0,2	3	0.0	0.0	$+2D_2^{pp}$	+1/4
					0.0	0.0	$-2D_2^{pp}$	+1/4
					0.0	0.0	0.0	−1/2
p_x	p_y	2	−2	4	$+D_2^{pp}$	$+D_2^{pp}$	0.0	+1/4
					$-D_2^{pp}$	$-D_2^{pp}$	0.0	+1/4
					$+D_2^{pp}$	$-D_2^{pp}$	0.0	−1/4
					$-D_2^{pp}$	$+D_2^{pp}$	0.0	−1/4
p_x	p_z	2	1	4	$+D_2^{pp}$	0.0	$+D_2^{pp}$	+1/4
					$-D_2^{pp}$	0.0	$-D_2^{pp}$	+1/4
					$+D_2^{pp}$	0.0	$-D_2^{pp}$	−1/4
					$-D_2^{pp}$	0.0	$+D_2^{pp}$	−1/4
p_y	p_z	2	−1	4	0.0	$+D_2^{pp}$	$+D_2^{pp}$	+1/4
					0.0	$-D_2^{pp}$	$-D_2^{pp}$	+1/4
					0.0	$+D_2^{pp}$	$-D_2^{pp}$	−1/4
					0.0	$-D_2^{pp}$	$+D_2^{pp}$	−1/4

(16)) and the electric field gradient (Eq. (17)) at a point in space **r** that can be calculated from a mulitpole expansion.

$$\mathrm{MEP}(\mathbf{r}) = Tq - T_\alpha\hat{\mu}_\alpha + \frac{1}{3}T_{\alpha\beta}\hat{\Theta}_{\alpha\beta} - \cdots + \frac{(-1)^n}{(2n-1)!!}T^{(n)}_{\alpha\beta\ldots\omega}\hat{\xi}^{(n)}_{\alpha\beta\ldots\omega} \quad (15)$$

$$F_\alpha(\mathbf{r}) = -\nabla_\alpha\,\mathrm{MEP}(\mathbf{r}) = -T_\alpha q + T_{\alpha\beta}\hat{\mu}_\beta + \frac{1}{3}T_{\alpha\beta\gamma}\hat{\Theta}_{\beta\gamma} - \cdots + \frac{(-1)^n}{(2n-1)!!}T^{(n+1)}_{\alpha\beta\ldots\psi\omega}\hat{\xi}^{(n)}_{\beta\gamma\ldots\psi\omega} \quad (16)$$

Table 2 (Contd.)

μ	ν	l	m	N	x	y	z	q
p_z	d_{z^2}	1	0	2	0.0	0.0	$+2\ D_1^{pd}$	$\sqrt{4/3}$
p_z	d_{xz}	1	1	2	$+2\ D_1^{pd}$	0.0	0.0	$+1$
p_z	d_{yz}	1	-1	2	0.0	$+2\ D_1^{pd}$	0.0	$+1$
p_x	d_{z^2}	1	1	2	$+2\ D_1^{pd}$	0.0	0.0	$-\sqrt{1/3}$
p_x	d_{xz}	1	0	2	0.0	0.0	$+2\ D_1^{pd}$	$+1$
p_x	$d_{x^2-y^2}$	1	1	2	$+2\ D_1^{pd}$	0.0	0.0	$+1$
p_x	d_{xy}	1	-1	2	0.0	$+2\ D_1^{pd}$	0.0	$+1$
p_y	d_{z^2}	1	-1	2	0.0	$+2\ D_1^{pd}$	0.0	$-\sqrt{1/3}$
p_y	d_{yz}	1	0	2	0.0	0.0	$+2\ D_1^{pd}$	$+1$
p_y	$d_{x^2-y^2}$	1	-1	2	0.0	$+2\ D_1^{pd}$	0.0	-1
p_y	d_{xy}	1	1	2	$+2\ D_1^{pd}$	0.0	0.0	$+1$
d_{z^2}	d_{z^2}	0	0	1	0.0	0.0	0.0	$+1$
		2	0	6	0.0	0.0	$+\sqrt{2}\ D_2^{dd}$	(4/3) (+1/4)
					0.0	0.0	$-\sqrt{2}\ D_2^{dd}$	(4/3) (+1/4)
					$+\sqrt{2}\ D_2^{dd}$	0.0	0.0	(4/3) (−3/8)
					$-\sqrt{2}\ D_2^{dd}$	0.0	0.0	(4/3) (−3/8)
					0.0	$+\sqrt{2}\ D_2^{dd}$	0.0	(4/3) (+1/8)
					0.0	$-\sqrt{2}\ D_2^{dd}$	0.0	(4/3) (+1/8)
d_{z^2}	d_{xz}	2	1	4	$+D_2^{dd}$	0.0	$+D_2^{dd}$	$\sqrt{1/3}$ (+1/4)
					$-D_2^{dd}$	0.0	$-D_2^{dd}$	$\sqrt{1/3}$ (+1/4)
					$+D_2^{dd}$	0.0	$-D_2^{dd}$	$\sqrt{1/3}$ (−1/4)
					$-D_2^{dd}$	0.0	$+D_2^{dd}$	$\sqrt{1/3}$ (−1/4)
d_{z^2}	d_{yz}	2	-1	4	0.0	$+D_2^{dd}$	$+D_2^{dd}$	$\sqrt{1/3}$ (+1/4)
					0.0	$-D_2^{dd}$	$-D_2^{dd}$	$\sqrt{1/3}$ (+1/4)
					0.0	$+D_2^{dd}$	$-D_2^{dd}$	$\sqrt{1/3}$ (−1/4)
					0.0	$-D_2^{dd}$	$+D_2^{dd}$	$\sqrt{1/3}$ (−1/4)
d_{z^2}	$d_{x^2-y^2}$	2	2	4	$+\sqrt{2}\ D_2^{dd}$	0.0	0.0	$-\sqrt{4/3}$ (+1/4)
					$-\sqrt{2}\ D_2^{dd}$	0.0	0.0	$-\sqrt{4/3}$ (+1/4)
					0.0	$+\sqrt{2}\ D_2^{dd}$	0.0	$-\sqrt{4/3}$ (−1/4)
					0.0	$-\sqrt{2}\ D_2^{dd}$	0.0	$-\sqrt{4/3}$ (−1/4)
d_{z^2}	d_{xy}	2	-2	4	$+D_2^{dd}$	$+D_2^{dd}$	0.0	$-\sqrt{4/3}$ (+1/4)
					$-D_2^{dd}$	$-D_2^{dd}$	0.0	$-\sqrt{4/3}$ (+1/4)
					$+D_2^{dd}$	$-D_2^{dd}$	0.0	$-\sqrt{4/3}$ (−1/4)
					$-D_2^{dd}$	$+D_2^{dd}$	0.0	$-\sqrt{4/3}$ (−1/4)
d_{xz}	d_{xz}	0	0	1	0.0	0.0	0.0	$+1$
		2,2	2,0	6	0.0	0.0	$+\sqrt{2}\ D_2^{dd}$	$+1/6$
					0.0	0.0	$-\sqrt{2}\ D_2^{dd}$	$+1/6$
					$+\sqrt{2}\ D_2^{dd}$	0.0	0.0	0
					$-\sqrt{2}\ D_2^{dd}$	0.0	0.0	0
					0.0	$+\sqrt{2}\ D_2^{dd}$	0.0	$-1/6$
					0.0	$-\sqrt{2}\ D_2^{dd}$	0.0	$-1/6$
d_{xz}	d_{yz}	2	-2	4	$+D_2^{dd}$	$+D_2^{dd}$	0.0	$+1/4$
					$-D_2^{dd}$	$-D_2^{dd}$	0.0	$+1/4$
					$+D_2^{dd}$	$-D_2^{dd}$	0.0	$-1/4$
					$-D_2^{dd}$	$+D_2^{dd}$	0.0	$-1/4$
d_{xz}	$d_{x^2-y^2}$	2	1	4	$+D_2^{dd}$	0.0	$+D_2^{dd}$	$+1/4$
					$-D_2^{dd}$	0.0	$-D_2^{dd}$	$+1/4$
					$+D_2^{dd}$	0.0	$-D_2^{dd}$	$-1/4$
					$-D_2^{dd}$	0.0	$+D_2^{dd}$	$-1/4$
d_{xz}	d_{xy}	2	-1	4	0.0	$+D_2^{dd}$	$+D_2^{dd}$	$+1/4$
					0.0	$-D_2^{dd}$	$-D_2^{dd}$	$+1/4$
					0.0	$+D_2^{dd}$	$-D_2^{dd}$	$-1/4$
					0.0	$-D_2^{dd}$	$+D_2^{dd}$	$-1/4$
d_{yz}	d_{yz}	0	0	1	0.0	0.0	0.0	$+1$
		2	0	6	0.0	0.0	$+\sqrt{2}\ D_2^{dd}$	$+1/6$
					0.0	0.0	$-\sqrt{2}\ D_2^{dd}$	$+1/6$
					$+\sqrt{2}\ D_2^{dd}$	0.0	0.0	$-1/2$
					$-\sqrt{2}\ D_2^{dd}$	0.0	0.0	$-1/2$
					0.0	$+\sqrt{2}\ D_2^{dd}$	0.0	$+1/3$
					0.0	$-\sqrt{2}\ D_2^{dd}$	0.0	$+1/3$

Table 2 (Contd.)

μ	ν	l	m	N	x	y	z	q
d_{yz}	$d_{x^2-y^2}$	2	−1	4	0.0	$+D_2^{dd}$	$+D_2^{dd}$	(−1) (+1/4)
					0.0	$-D_2^{dd}$	$-D_2^{dd}$	(−1) (+1/4)
					0.0	$+D_2^{dd}$	$-D_2^{dd}$	(−1) (−1/4)
					0.0	$-D_2^{dd}$	$+D_2^{dd}$	(−1) (−1/4)
d_{yz}	d_{xy}	2	1	4	$+D_2^{dd}$	0.0	$+D_2^{dd}$	+1/4
					$-D_2^{dd}$	0.0	$-D_2^{dd}$	+1/4
					$+D_2^{dd}$	0.0	$-D_2^{dd}$	−1/4
					$-D_2^{dd}$	0.0	$+D_2^{dd}$	−1/4
$d_{x^2-y^2}$	$d_{x^2-y^2}$	0	0	1	0.0	0.0	0.0	+1
		2	0	6	0.0	0.0	$+\sqrt{2}\ D_2^{dd}$	(−4/3) (+1/4)
					0.0	0.0	$-\sqrt{2}\ D_2^{dd}$	(−4/3) (+1/4)
					$+\sqrt{2}\ D_2^{dd}$	0.0	0.0	(−4/3) (−3/8)
					$-\sqrt{2}\ D_2^{dd}$	0.0	0.0	(−4/3) (−3/8)
					0.0	$+\sqrt{2}\ D_2^{dd}$	0.0	(−4/3) (+1/8)
					0.0	$-\sqrt{2}\ D_2^{dd}$	0.0	(−4/3) (+1/8)
d_{xy}	d_{xy}	0	0	1	0.0	0.0	0.0	+1
		2	0	6	0.0	0.0	$+\sqrt{2}\ D_2^{dd}$	(−4/3) (+1/4)
					0.0	0.0	$-\sqrt{2}\ D_2^{dd}$	(−4/3) (+1/4)
					$+\sqrt{2}\ D_2^{dd}$	0.0	0.0	(−4/3) (−3/8)
					$-\sqrt{2}\ D_2^{dd}$	0.0	0.0	(−4/3) (−3/8)
					0.0	$+\sqrt{2}\ D_2^{dd}$	0.0	(−4/3) (+1/8)
					0.0	$-\sqrt{2}\ D_2^{dd}$	0.0	(−4/3) (+1/8)

$$F_{\alpha\beta}(\mathbf{r}) = -\nabla_\alpha \nabla_\beta \,\mathrm{MEP}(\mathbf{r}) = -T_{\alpha\beta} q + T_{\alpha\beta\gamma}\hat{\mu}_\gamma + \frac{1}{3} T_{\alpha\beta\gamma\delta}\hat{\Theta}_{\gamma\delta} - \cdots + \frac{(-1)^n}{(2n-1)!!} T^{(n+2)}_{\alpha\beta\ldots\chi\psi\omega}\hat{\xi}^{(n)}_{\gamma\delta\ldots\chi\psi\omega} \tag{17}$$

with

$$T = \frac{1}{R} \tag{18}$$

$$T_\alpha = \nabla_\alpha \frac{1}{R} = -\frac{R_\alpha}{R^3} \tag{19}$$

$$T_{\alpha\beta} = \nabla_\alpha \nabla_\beta \frac{1}{R} = \frac{3\,R_\alpha R_\beta - R^2\delta_{\alpha\beta}}{R^5} \tag{20}$$

$$T_{\alpha\beta\gamma} = \nabla_\alpha \nabla_\beta \nabla_\gamma \frac{1}{R} = -\frac{15\,R_\alpha R_\beta R_\gamma - 3R^2(R_\alpha \delta_{\beta\delta} + R_\beta \delta_{\alpha\gamma} + R_\gamma \delta_{\alpha\beta})}{R^7} \tag{21}$$

$$\begin{aligned} T_{\alpha\beta\gamma\delta} &= \nabla_\alpha \nabla_\beta \nabla_\gamma \nabla_\delta \frac{1}{R} \\ &= \frac{1}{R^9}[105\,R_\alpha R_\beta R_\gamma R_\delta \\ &\quad -15\,R^2(R_\alpha R_\beta \delta_{\gamma\delta} + R_\alpha R_\gamma \delta_{\beta\delta} + R_\alpha R_\delta \delta_{\beta\gamma} \\ &\quad + R_\beta R_\gamma \delta_{\alpha\delta} + R_\beta R_\delta \delta_{\alpha\gamma} + R_\gamma R_\delta \delta_{\alpha\beta}) \\ &\quad + 3R^4(\delta_{\alpha\beta}\delta_{\gamma\delta} + \delta_{\alpha\gamma}\delta_{\beta\delta} + \delta_{\alpha\delta}\delta_{\beta\gamma})]. \end{aligned} \tag{22}$$

References

1. Stone AJ (2002) The theory of intermolecular forces, chapter 2. Clarendon Press, Oxford, p 12
2. Politzer P, Murray JS (1998) Molecular electrostatic potentials and chemical reactivity. In: Lipkowitz K, Boyd RB (eds), Rev Comput Chem, vol 2. VCH, New York pp 273–312
3. Murray JS, Politzer P (2003) The use of the molecular electrostatic potential in medicin chemistry. In: Carloni P, Alber F, Mannhold R, Kubinyi H, Folkers G (eds), Quantum medicinal chemistry, vol 17. Wiley-VCH, New York pp 233–254
4. Ehresmann B, de Groot MJ, Alex A, Clark T (2004) J Chem Inf Comput Sci 43:658–668
5. Podlipnik Č, Koller J (1998) Croat Chem Acta 71:689–696
6. Reynolds CA, Richards WG, Goodford PJ (1988) J Chem Soc Perkin Trans II, pp 551–556
7. Miertuš S, Scrocco E, Tomasi J (1981) J Chem Soc Perkin Trans pp 1439–1443
8. Wong MW, Frisch MJ, Wiberg KB (1991) J Am Chem Soc 113:4776–4782
9. Rauhut G, Clark T, Steinke T (1993) J Am Chem Soc 115:9174–9181
10. Zou J, Yu Y, Shang Z (2001) J Chem Soc Perkin Trans pp 1439–1443
11. Dewar MJS, Thiel W (1977) J Am Chem Soc 99:4899–4907
12. Dewar MJS, Zoebisch EG, Healy EF, Stewart JJP (1985) J Am Chem Soc 107:3902–3909
13. Stewart JJP (1989) J Comput Chem 10:209–220
14. Beck B, Horn A, Carpenter J, Clark T (1998) J Chem Inf Comput Sci 38:1214–1217
15. Rein R (1973) Adv Quantum Chem 7:335–396
16. Merz KM, Besler BH (1990) QCPE Bull 10:15
17. Reynolds CA, Ferenczy GG, Richards WG (1992) J Mol Struct (Theochem) 256:249–269
18. Parr RG (1960) J Chem Phys 33:1184–1199
19. Ford GP, Wang B (1993) Ab Initio hf/6-31g* results. J Comput Chem 14:1101–1111
20. Bakowies D, Thiel W (1996) J Comput Chem 17:87–108
21. Dewar MJS, Thiel W (1977) Theor Chim Acta 46:89–104

22. Rauhut G, Clark T (1993) J Comput Chem 14:503–509
23. Beck B, Rauhut G, Clark T (1994) J Comput Chem 15:1064–1073
24. Göller AH, Horn AHC, Clark T (unpublished)
25. Horn AHC (2004) PhD Thesis, Friedrich-Alexander-Universität Erlangen-Nürnberg
26. Löwdin PO (1995) Phys Rev 97:1474–1489 DOI 10.1103 Phys Rev 971490
27. Gedeck P, Schindler T, Alex A, Clark T (2000) J Mol Model 6:452–466
28. Thiel W, Voityuk AA (1992) Theor Chim Acta 81:391–404
29. Thiel W, Voityuk AA (1996) Theor Chim Acta 93:315
30. Pople JA, Beveridge DL (1970) Approximate molecular orbital theory. McGraw-Hill, New York
31. Roothaan CCJ (1951) J Chem Phys 19:1445–1458
32. Pople JA, Santry DP (1965) J Chem Phys 43:S129–S135
33. Klopman G (1964) J Am Chem Soc 86:4550–4557
34. Stone AJ (2002) The theory of intermolecular forces, chapter 2. Clarendon Press, Oxford pp 12–18
35. Stone AJ (2002) The theory of intermolecular forces, chapter 3. Clarendon Press, Oxford pp 36–38
36. Clark T, Alex A, Beck B, Burkhardt F, Chandrasekhar J, Gedeck P, Horn AHC, Hutter M, Martin B, Rauhut G, Sauer W, Schindler T, Steinke T (2004) VAMP 8.1. Erlangen
37. Winget P, Horn AHC, Selçuki C, Martin B, Clark T (2003) J Mol Model 9:408–414
38. Stephens PJ, Devlin FJ, Chabalowski CF, Frisch MJ (1994) J Phys Chem 98:11623–11627
39. Becke AD (1996) J Chem Phys 104:1040–1046
40. Møller C, Plesset MS (1934) Phys Rev 46:618–622
41. Head-Gordon M, Pople JA, Frisch MJ (1988) Chem Phys Lett 153:503–506
42. Frisch MJ, Head-Gordon M, Pople JA (1990) Chem Phys Lett 166:275–280
43. Frisch MJ, Head-Gordon M, Pople JA (1990) Chem Phys Lett 166:281–289
44. Frisch MJ, Pople JA, Binkley JS (1984) J Chem Phys 80:3265–3269
45. Hehre WJ, Ditchfield R, Pople JA (1972) J Chem Phys 56:2257–2261
46. McLean AD, Chandler GS (1980) J Chem Phys 72:5639–5648
47. Hay PJ, Wadt WR (1985) J Chem Phys 82:270–283
48. Wadt WR, Hay PJ (1985) J Chem Phys 82:284–298
49. Hay PJ, Wadt WR (1985) J Chem Phys 82:299–310
50. Extra polarization functions consisted of one unscaled Gaussian with the following Gaussian exponents α for each function type ("shell"): Mo: p function, $\alpha_p = 1$; f function, $\alpha_f = 0.072$; all prefactors were set to 1.0
51. Frisch MJ, Trucks GW, Schlegel HB, Scuseria GE, Robb MA, Cheeseman JR, Montgomery JA, Jr, Vreven T, Kudin KN, Burant JC, Millam JM, Iyengar SS, Tomasi J, Barone V, Mennucci B, Cossi M, Scalmani G, Rega N, Petersson GA, Nakatsuji H, Hada M, Ehara M, Toyota K, Fukuda R, Hasegawa J, Ishida M, Nakajima T, Honda Y, Kitao O, Nakai H, Klene M, Li X, Knox JE, Hratchian HP, Cross JB, Adamo C, Jaramillo J, Gomperts R, Stratmann RE, Yazyev O, Austin AJ, Cammi R, Pomelli C, Ochterski JW, Ayala PY, Morokuma K, Voth GA, Salvador P, Dannenberg JJ, Zakrzewski VG, Dapprich S, Daniels AD, Strain MC, Farkas O, Malick DK, Rabuck AD, Raghavachari K, Foresman JB, Ortiz JV, Cui Q, Baboul AG, Clifford S, Cioslowski J, Stefanov BB, Liu G, Liashenko A, Piskorz P, Komaromi I, Martin RL, Fox DJ, Keith T, Al-Laham MA, Peng CY, Nanayakkara A, Challacombe M, Gill PMW, Johnson B, Chen W, Wong MW, Gonzalez C, Pople JA (2003) Gaussian 03, Revision B.03. Gaussian, Inc., Pittsburgh
52. Carbo R, Leyda L, Arnau M (1980) Int J Quant Chem 17:1185–1189
53. Hodgkin EE, Richards GW (1987) Int J Quant Chem 14:105–110
54. Winget P, Selçuki C, Horn AHC, Martin B, Clark T (2003) Theor Chem Acc 110:254–266
55. Beck B, Glenn RC, Clark T (1995) J Mol Model 1:176–187
56. Beck B, Glenn RC, Clark T (1997) J Comput Chem 18:744–756
57. Klamt A, Schüürmann G (1993) J Chem Soc Perkin Trans 2, pp 799–805
58. Andzelm J, Kölmel C, Klamt A (1995) J Chem Phys 103:9312–9320
59. Klamt A In Schleyer PvR, Allinger NL, Clark T, Gasteiger J, Kollman PA, Schaefer HF, III, Schreiner PR, editors, Encyclopedia of Computational Chemistry, volume 1, pages 604–615. Wiley, Chichester, UK, 1998

Note added in proof:

After this manuscript was in the press, we became aware of an existing implementation of the mthod described here in the COSMO solvent model [57] code of Mopac 7 for the standard NDDO sp-basis (i.e. without d-orbitals).

For completeness, we include two additional references [58,59] that refer to this implementation without defining it completely or testing its performance.